frontiers in Materials

ORIGINAL RESEARCH
published: 07 July 2020
doi: 10.3389/fmats.2020.00192

Surface Structure and Phase Composition of TiO_2 P25 Particles After Thermal Treatments and HF Etching

M. Jasim Uddin[1], Federico Cesano[2], Aminur Rashid Chowdhury[1], Tarek Trad[3], Sara Cravanzola[2], Gianmario Martra[2], Lorenzo Mino[2], Adriano Zecchina[2] and Domenica Scarano[2]**

[1] PERL-Photonics and Energy Research Laboratory, Department of Chemistry, University of Texas Rio Grande Valley, Edinburg, TX, United States, [2] Department of Chemistry, NIS-Nanostructured Interfaces and Surfaces, Inter-Departmental Centre and INSTM Centro di Riferimento, University of Torino, Turin, Italy, [3] Department of Chemistry, Sam Houston State University, Huntsville, TX, United States

The anatase to rutile phase transformation via thermal and chemical (HF etching) routes of TiO_2 P25 has been investigated. The treatment parameters and properties of the resulting anatase and rutile nanoparticles are analyzed and discussed. Since the nature of TiO_2 surfaces plays a significant role in determining the physical and chemical properties of the TiO_2 nanoparticles, it is important to investigate the surface properties, including the morphology, the main exposed faces, the defectiveness, to be correlated with their peculiar properties, and then reactivity. Herein, we report an infrared spectroscopy investigation, employing the adsorption of CO probe molecule at low temperature, including ^{12}CO and ^{12}CO-^{13}CO isotopic mixtures, at the surface sites of TiO_2 P25, previously heated from room temperature to 1,023 K under vacuum conditions. The same FTIR experiments were adopted on HF-etched TiO_2. X-ray diffraction and transmission electron microscopy analyses were adopted to elucidate the role played by the thermal and the HF-etching treatments in modifying not only the distribution of exposed surfaces, but even the phase composition of the pristine TiO_2 P25 samples, which are initially dominated by the most thermodynamically stable (101) facets of the anatase phase. The present study helps in the crystal and exposed facet engineering for the development of highly efficient photocatalysts.

Keywords: TiO_2, P25, thermal treatment, HF etching, FTIR, HRTEM, XRD, surface properties

OPEN ACCESS

Edited by:
P. Davide Cozzoli, University of Salento, Italy

Reviewed by:
Avelino Corma, Universitat Politècnica de València, Spain
Michael Nolan, University College Cork, Ireland

****Correspondence:***
M. Jasim Uddin
mohammed.uddin@utrgv.edu
Domenica Scarano
domenica.scarano@unito.it

Specialty section:
This article was submitted to Colloidal Materials and Interfaces, a section of the journal Frontiers in Materials

Received: *03 February 2020*
Accepted: *25 May 2020*
Published: *07 July 2020*

Citation:
Uddin MJ, Cesano F, Chowdhury AR, Trad T, Cravanzola S, Martra G, Mino L, Zecchina A and Scarano D (2020) Surface Structure and Phase Composition of TiO_2 P25 Particles After Thermal Treatments and HF Etching. Front. Mater. 7:192. doi: 10.3389/fmats.2020.00192

INTRODUCTION

Titanium dioxide (TiO_2) is a multifunctional material that is a matter of interest in a wide range of applications, ranging from the photocatalysis to energy fields (Qadir et al., 2016; Jaksik et al., 2017; Cravanzola et al., 2018; Humayun et al., 2018; Tamgadge and Shukla, 2018; Hussain et al., 2019). TiO_2 nanoparticles can be obtained by different preparation methods, including sol-gel methods, hydrothermal treatments, and flame spray pyrolysis. Along this line, TiO_2 crystals prepared by flame hydrolysis of $TiCl_4$ reveal a nearly perfect crystalline habit and can be substantially different from samples prepared by wet-chemistry pathways. For example, TiO_2 P25 powders from Evonik, are prepared following the flame pyrolysis. As a result of this procedure, the obtained

TiO_2 nanocrystals show the most thermodynamically stable (101) surface (Diebold et al., 2003; Mino et al., 2011) and (100)/(010) surface planes, together with some more reactive (001) facets (Vittadini et al., 1998; Yang et al., 2008; Mino et al., 2012, 2013, 2016; Deiana et al., 2013a). Otherwise, crystallinity, sizes of TiO_2 nanoparticles, obtained by other synthetic procedures, can differ remarkably (Djaoued et al., 2002; Uddin et al., 2007; Daoud and Xin, 2008; Liu et al., 2018) and the crystal habits can significantly differ with preparation techniques (Diebold et al., 2003). As the morphology has a significant impact on the physical chemical properties, it is clear that the choice of a specific TiO_2 material and the approaches to modify the properties of a well-known TiO_2 polytype are mandatory. The strategies include the particle-size and morphology control (Yang et al., 2008; Liu et al., 2011), the self-assembly (Cesano et al., 2008; Likodimos, 2018), the combination with other phases or structures (Cesano et al., 2012, 2015; Jain et al., 2014; Grissom et al., 2018), the TiO_2 doping with metal/non-metal elements (Cravanzola et al., 2017; Humayun et al., 2018), as well as the embedding of quantum dots, heteroatoms, or heterostructures (Chen and Mao, 2007; Uddin et al., 2014; Jia et al., 2019) for tuning the optical and electronic properties.

The anatase TiO_2, by far the most recognized photoactive polytype, is dominated by the utmost thermodynamically stable (101) facets (>94%) in agreement with the Wulff construction, in preference to the much more reactive (001) ones. The control of the morphology and then of the extension of the other high-energy surfaces has been shown in the work of Yang et al. (2008) and Selloni (2008). According to the authors, the crystals growth, with a high percentage (about 47%) of (001) facets, has been obtained by employing HF as a shape controller. Along this, newly developed procedures based on HF/alcohol mixtures under hydrothermal conditions have been employed for stabilizing a larger quantity of reactive (metastable) surfaces, till to reach about 98.7% and 1.3% of (001) and (100) facets, respectively (Wen et al., 2011). Notably, curved TiO_2 crystals, exposing continuous curvature on the crystal surface of both the anatase and rutile, have been more recently obtained by using F^- together with citric acid or other hydroxyl acids, whose role as capping agents at specific facets under hydrothermal conditions, has been shown (Yang et al., 2014). The multiple role played by F^- as a stabilizer for the (001) facet growth and as an etching reagent has been suggested by considering also the most recent papers (Zhang et al., 2011; Yang et al., 2014; Jiwei Ma et al., 2017; Liu et al., 2018; Mino et al., 2018; Peng et al., 2018; Zou et al., 2018). Taking into account all these works (Yang et al., 2008; Wen et al., 2011), it comes out that H_2O and F^- concentrations are competitive factors in affecting the morphology of anatase nanoparticles (Jiwei Ma et al., 2017). As a matter of fact, hydroxyl groups promote the isotropic growth of crystals, while F-terminated (001) surfaces favor the lateral growth of TiO_2 crystals. Furthermore, it is also shown that the particle size can be significantly reduced at the very high F^- concentrations, due to the formation of soluble titanium fluoride or $TiOF_2$. Along these themes, we can take advantage of the simple HF etching effects on commercial TiO_2 systems, such as P25 powder that contains nanocrystals of anatase and rutile in the 80:20 weight ratio. It has been shown that, depending on the hydrothermal conditions (i.e., pH, HF concentration and then type of etching conditions, time, temperature, and pressure) (Jiwei Ma et al., 2017), the stepping of (101) surface (Deiana et al., 2013b), or alternatively the selective etching of the anatase phase can be obtained (Mino et al., 2013).

Although the structure of the surface can be investigated by using microscopy techniques, including electron and scanning tunneling microscopies, details concerning the surface sites of TiO_2 polytypes still remain elusive. In general, an accurate and deep understanding of the active sites, their Lewis acidity, coordination states, including local defects and more extended terminations at the surface, can be gained by adsorption of small molecular probes (Mino et al., 2014, 2019; Zaera, 2014; Cravanzola et al., 2017), like CO (Desjonqueres and Spanjaard, 1996; Hadjiivanov and Klissurski, 1996; Scarano et al., 2004; Groppo et al., 2006). In this contest, we report a Fourier-transform infrared (FTIR) spectroscopic study of the surface sites present on TiO_2 P25 treated at different temperatures (RT, 473, 673, 773, 873, 973, and 1,023 K) or etched with HF solutions at different level of concentrations. In this investigation, the CO molecules are used as surface probes before and after HF etching reactions to give further contributions to the knowledge of the surface chemistry. X-ray diffraction (XRD) and transmission electron microscopy (TEM) analyses were adopted to elucidate the role played by the thermal and the HF-etching treatments.

EXPERIMENTAL

Materials

Commercial TiO_2 (Evonik P25), having about 50 m^2g^{-1} as surface area, was used without any further modification throughout the experiments.

Methods

X-ray diffraction patterns of TiO_2 powders were obtained, after the thermal activation treatments in vacuum and FTIR experiments, by means of a Philips PW1830/PW1050 diffractometers, working in a Bragg-Brentano geometry and with a $Co_{K\alpha}$ radiation (1.7890 Å). Quantitative analyses of anatase **(A)** and rutile (R) phases were carried out by means of the following equation (Spurr and Myers relationship) (Spurr and Myers, 1957): $A_{(wt\%)} = 1/(1+ 1.265\cdot(I_R/I_A))\times 100$, where I_A and I_R correspond to the integrated intensities of anatase (101) and (110) rutile reflections located at 29.4° and at 32.0°, respectively. The same XRD reflections were also used to calculate the average crystallite sizes by using the Scherrer equation: $L = \kappa\ \lambda/(\beta\text{-}\beta_i)\ \cos\theta$, where L is the crystal size domain, $\kappa = 0.9$, β is the observed FWHM and β_i is the calculated instrumental broadening.

Transmission electron microscopy (TEM) images of TiO_2 powders were obtained by means of a JEOL 3010-UHR instrument operating at 300 kV with a point-to point resolution of 0.12 nm and equipped with a 2k × 2k pixels Gatan US1000 CCD camera. Powders were placed dry on a lacey carbon coated copper grid without solvent.

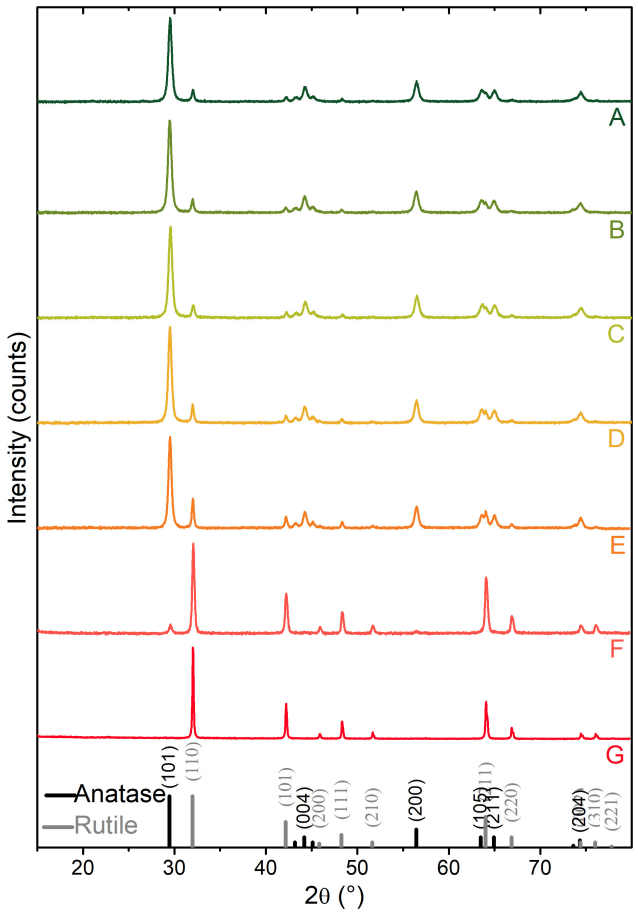

FIGURE 1 | XRD patterns of TiO_2 P25 powders: **(A)** outgassed at RT, **(B–G)** thermally treated at 473, 673, 773, 873, 973, 1,023 K activation temperatures, respectively. Peak positions and relative intensities (vertical lines) of anatase (PDF card #21-1272) and rutile TiO_2 (PDF card #21-1276) are shown for comparison.

TiO_2 samples have been obtained in form of thin self-supporting pellets for IR transmission experiments. The IR spectra were recorded with IFS 28 FTIR spectrophotometer having a resolution of 2 cm^{-1}. An IR cell which has been specially constructed for the low-temperature measurements (ca. 100 K), was equipped with a vacuum line allowing to ensure a vacuum $\leq 10^{-4}$ mbar and then to dose CO gas in a controlled way. Self-supported thin pellets were activated in the IR cell by outgassing (1 h) and then thermally treated under oxygen (1 h, P_{O2} = 50 mbar) at 473, 673, 773, 873, 973, or 1,023 K. Chemical etching was carried out by immersing the TiO_2 powder in 1 and 6 vol% HF solutions for 1 h and in a 10 vol% HF solution for 12 h (hereafter HF-TiO_2). After chemical etching, HF-TiO_2 powders were separated by centrifugation, washed with deionized water and heated in air at 773 K for 1 h to eliminate all residual F species present after the HF treatment. The HF-TiO_2 samples were measured at 60 K using an Oxford CCC 1204 cryostat properly modified to fit in the sample compartment of the FTIR spectrophotometer (Mino et al., 2012, 2013).

TABLE 1 | Phase composition and crystal size analysis from XRD patterns shown in **Figure 1**.

Temperature of treatments[a]	Phase composition[b]		Crystallite sizes[c]	
	Anatase (wt%)	Rutile (wt%)	Anatase (nm)	Rutile (nm)
RT	83	17	28	47
473 K	83	17	28	47
673 K	83	17	28	47
773 K	80	20	33	56
873 K	59	41	35	60
973 K	7	93	48	62
1,023 K		100		237

[a] *Activation treatments: under vacuum ($\leq 10^{-4}$ mbar) for 1 h then oxidation with O_2 (15 mbar) for 1 h.*
[b] *Calculated by Spurr and Myers relation (see Methods).*
[c] *Calculated by Scherrer's equation (see Methods).*

RESULTS AND DISCUSSION

XRD Analysis: Phase Composition and Crystal Sizes

X-ray diffraction patterns of TiO_2 P25, obtained after thermal activation in vacuum at different temperatures from RT to 1,023 K are compared to the standard anatase (PDF card #21-1272) and rutile (PDF card #21-1276) (**Figure 1**).

XRD diffraction peaks at 2θ = 29.4°, 44.2°, 56.4°, 63.5°, 64.9°, and 74.3° match with (101), (004), (200), (105), (211), and (204) diffraction planes of anatase, while those located at 32.0°, 42.2°, 48.3°, 64.0°, 66.8°, and 76.0° are assigned to the (110), (101), (111), (211), (220), and (310) diffraction planes of rutile. Quantitative phase analysis and mean crystallite sizes of the thermally activated samples are reported in **Table 1**. More in detail, from the XRD pattern of the sample outgassed at RT made by 83 wt% of anatase and 17 wt% of rutile (A-pattern in **Figure 1**), mean crystallite sizes of about 28 and 47 nm for anatase and rutile nanoparticles, respectively, are obtained. Notice that phase compositions and crystallite size domains remain almost unaltered upon increasing the activation temperature up to 673 K (C-pattern in **Figure 1**). Conversely, the main peak of the rutile phase, located at 2θ = 32.0°, is progressively increasing in intensity, upon activation temperatures at 773, 873, 973, and 1,023 K, for 2 h (D–G patterns in **Figure 1**), which corresponds to a progressively increasing amount of rutile phase from 20 wt% up to 41 wt%, 93 wt%, and 100 wt%, respectively. The phase composition, together with the increasing crystallite sizes reported in **Table 1**, clearly indicates that, under the adopted conditions, the conversion from anatase to rutile is thermally activated, being entirely completed at the highest temperature (~1,023 K). Some more, the changes of the crystallographic phase due to the heat treatments take place together with sintering processes, as shown also from full-width-at-half-maximum (FWHM) of the XRD peaks. These results are not surprising and the anatase-to-rutile thermal conversion is well-documented in

literature (Chen and Mao, 2007; Kitano et al., 2008; Nolan et al., 2009; Hanaor and Sorrell, 2011; Byrne et al., 2016).

TEM and HRTEM Analysis: Structure and Morphology

Samples obtained at three selected temperatures of treatment (RT, 773 K and 1,023 K) were TEM imaged and the results are shown in **Figure 2**. Nanocrystals with a wide size distribution in the 10–40 nm range can be observed at the low resolution TEM image of the native TiO_2 P25 powder (**Figure 2A**). As observed from the high-resolution TEM (HRTEM) images, the nanoparticles are highly crystalline, but the size distribution is more broader with respect to shape-engineered TiO_2 nanoparticles, synthesized employing capping agents (Mino et al., 2018). An anatase nanoparticle is HRTEM imaged in **Figure 2B**. Such nanoparticle well-exhibits a periodicity in the real space with well-defined interference fringes 0.353 nm spaced corresponding to (101) and (011) planes of anatase, which show an array of bright spots in the reciprocal space (FFT image) as imaged from [111] zone axis (**Figure 2C**). Other higher indexed lattice fringes, such as (11–2) can be also identified from both HRTEM and FFT images. Such interference fringes can be observed parallelly oriented to the lateral sides of the anatase nanocrystal, indicating that they preferentially expose (101), and (110) surfaces.

Similar qualitative observations can be made for the TiO_2 sample activated at 773 K (**Figures 2D–F**). No remarkable variations in dimensions are observed at low resolution (**Figure 2D**), but atomic stepped edges and apparently high index facets can be noticed at the higher resolution. An anatase nanocrystal is HRTEM imaged in **Figure 2E**. In this image, a nanocrystal of ca. 20 nm shows well-defined interference fringes corresponding to anatase (101) and (011) planes imaged from the [111] zone axis (**Figure 2F**).

A remarkable variation in sizes can be observed for the sample treated at 1,023 K (**Figure 2G**). A HRTEM image of a nanoparticle exposing regular and sharp edges with well-defined interference fringes is shown in **Figure 2H**. The observed fringes are compatible with rutile (011) and (101) lattice planes as imaged from [−111] zone axis (**Figure 2I**).

In conclusions, in all the imaged samples the observed lattice fringes are always observed parallelly oriented to the external sides of the nanocrystals, indicating that they preferentially expose (101) and (110) surfaces.

FTIR Spectra of Adsorbed CO on TiO_2 Surface Activated at Different Temperature

FTIR spectra of CO adsorbed on TiO_2 surfaces represent a valuable tool for the investigation of the nature of the surface active sites and then of the particle morphology. As a matter of fact, the stretching frequency of the adsorbed CO (ν_{CO}) is very sensitive to the type and structure of the exposed faces. This means that the interaction of CO with cations, having either different activity and different local arrangement of the nearest neighbors on the exposed facets, would originate peculiar spectroscopic features (Cesano et al., 2010; Scarano et al., 2019).

FTIR spectra of CO adsorbed at 100 K on the TiO_2 surface of previously activated samples at increasing temperatures, from RT to 1,032 K have been investigated (**Figures 3A–G**).

The spectra are dominated at the maximum coverage ($\theta \rightarrow \sim 1$) by an intense band with maximum at ν = 2,178 cm^{-1}, which gradually increases in intensity upon increasing the activation temperature from RT up to 773 K (**Figures 3A–D**) and shifts upward to 2,189–2,190 cm^{-1} at decreasing CO coverage ($\theta \rightarrow 0$). The band, which is attributed to CO adsorbed on pentacoordinated Ti^{4+}, can be explained with the formation of a Ti^{+4} –CO (σ) bond, while the shifting with the coverage is indicative of the building up of lateral interactions within the adlayer of CO oscillators (dipole and static in nature) (Scarano et al., 1992). Notice that the absorption frequency of CO on sample outgassed at RT is not significantly affected by the CO coverage ($\Delta\nu$ <2 cm^{-1}) (**Figure 3A**), whereas the spectral features, observed for samples obtained upon increasing the outgassing temperature (**Figures 3B–E**), show a visible coverage-induced shifting from ∼2 to ∼12 cm^{-1} (2,178→2,190 cm^{-1} from $\theta \cong 1$ to $\theta = 0$).

All these observations indicate that the CO species adsorbing in the 2,178–2,192 cm^{-1} range are associated with an array of parallel CO oscillators adsorbed on flat surfaces or terraces. On the basis of data obtained on shape-controlled TiO_2 nanoparticles (Deiana et al., 2013a; Mino et al., 2018) and on TiO_2 single crystals (Xu et al., 2011), we can safely state that the responsible face is the anatase (101), which is the most stable.

Likewise, the weaker band at about 2,164 cm^{-1}, which is developing upon higher activation temperature (773 K) (**Figure 3D**), progressively shifts upward upon decreasing the coverage, being this behavior also indicative of the building-up of lateral interactions among CO oscillators adsorbed on Ti^{4+} sites at anatase (100) surfaces (Mino et al., 2018). Moreover, a minor component at 2,154–2,157 cm^{-1} have been also assigned to CO adsorbed on residual hydroxyl groups and on the minority anatase (001) facets (Tsyganenko et al., 1985; Cravanzola et al., 2018; Mino et al., 2018). It is noteworthy that the observed high reversibility and the small difference with respect to ν_{CO} (gas) indicate that Ti^{+4} centers on these terraces or facets have a low Lewis acidic character. The increase of the frequency shift with the activation temperature is likely associated with the decrement of hydroxyls concentration and with the associated increase of the extension of fully dehydroxylated and more regular patches, where adsorbate-adsorbate interaction can fully develop.

The evolution of the spectra obtained for samples treated at even higher temperatures (873 K, 973 K, and 1,023 K) (**Figures 3E–G**) can be interpreted with the contribution of rutile phase, which is progressively increasing. The reported spectra are dominated at the maximum coverage ($\theta \rightarrow \sim 1$) by more complex bands. As a matter of fact, the spectrum of the sample treated at 873 K (**Figure 3E**) shows at high CO coverage, beside the maximum at 2,178 cm^{-1}, a partially resolved shoulder at 2,185 cm^{-1} that can be assigned to CO adsorbed on Ti^{4+} sites at (110)/(112) surfaces of anatase (Deiana et al., 2010; Mino et al., 2012). The anatase phase is still prevailing, despite the increasing

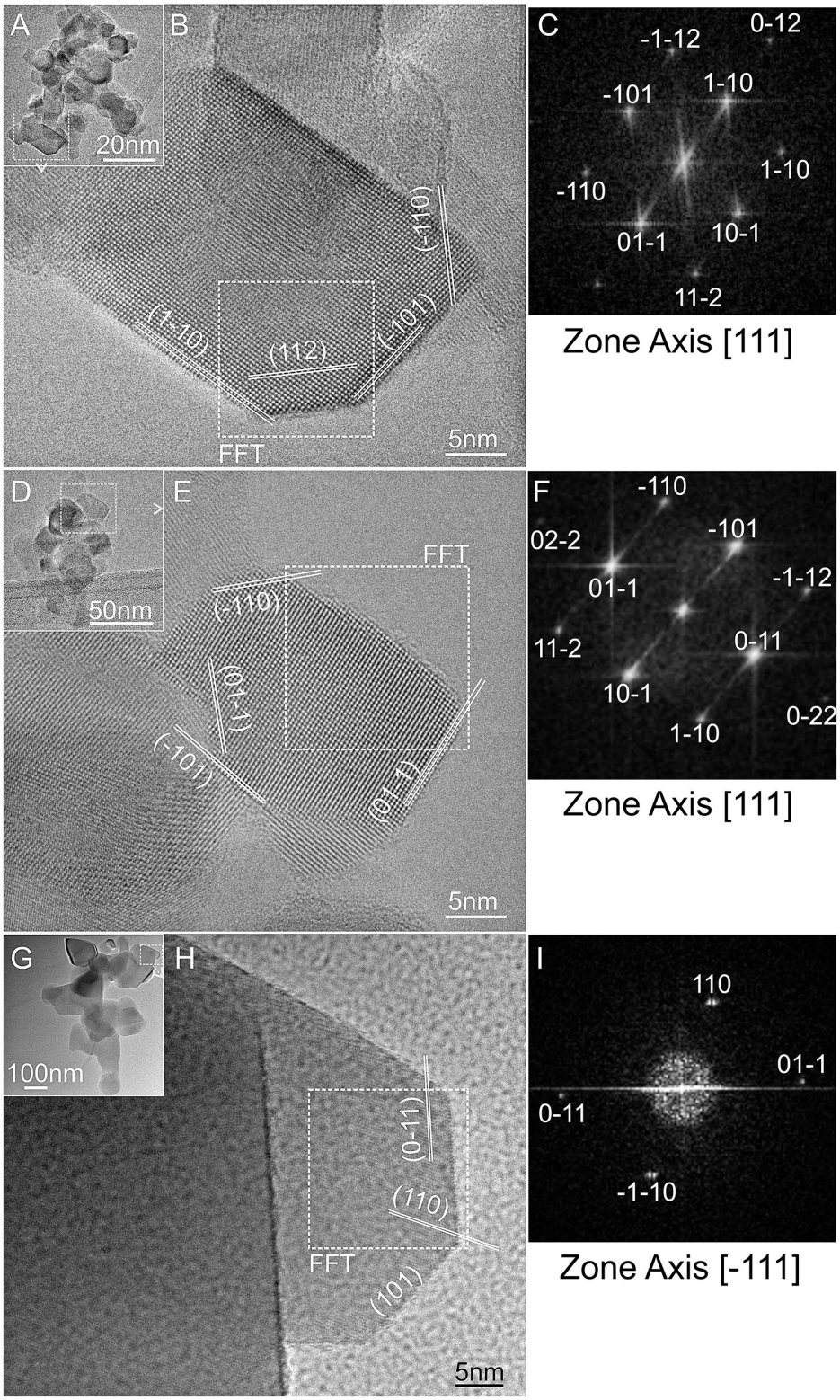

FIGURE 2 | TEM images and the related high-resolution TEM selected regions of: **(A,B)** TiO_2 P25, and of the same P25 powder after thermal activation in vacuum at: **(D,E)** 773 K and **(G,H)** 1,023 K; **(C,F,I)** fast-Fourier-transform (FFT) images of the selected nanocrystals in **(A,D,G)**, as obtained from [111] or [-111] zone axis directions.

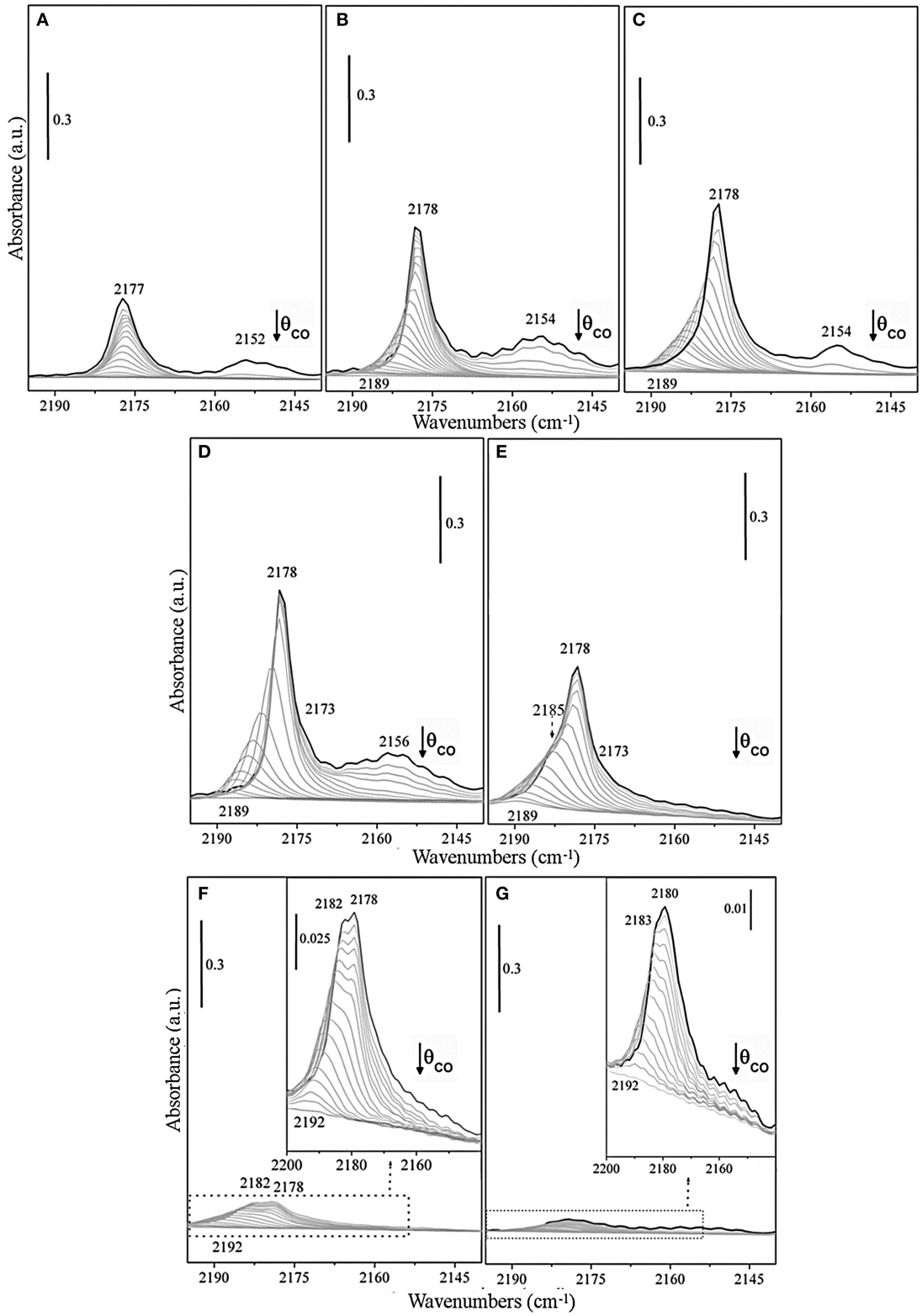

FIGURE 3 | FTIR spectra at 100 K of adsorbed CO (P_{CO} = 50 mbar) at decreasing coverages on TiO_2 (P25) surface, previously outgassed for 1 h, and successively treated at the same temperature for 1 h with static O_2 (P_{O2} = 50 mbar) at **(A)** RT, **(B)** 473 K, **(C)** 673 K, **(D)** 773 K, **(E)** 873 K, **(F)** 973 K, and **(G)** 1,023 K, respectively.

amount of rutile phase, being the last one about 41 wt%. An interesting observation is that no new features, attributable to CO on rutile can be clearly evidenced at this stage. The shoulder at 2,184 cm^{-1} appears to be stable at the early stages, then shifts upward at lower coverage. Therefore, this signal seems relatively less affected by the reduced CO–CO interactions, when compared to the main peak (2,178 cm^{-1}), as discussed in a previous study (Deiana et al., 2016).

Taken in consideration these findings, we can state that the role of rutile phase in affecting the CO spectra of samples outgassed at T $\leq$773 K is not evident and hence the contribution of CO adsorbed on rutile surface is very low, in agreement with the XRD data reported in **Table 1**.

Actually, moving to the spectra of the sample treated at 973 K (**Figure 3F**), a broad envelope made by a shoulder at 2,182 cm^{-1} and a wide band with maximum at 2,178 cm^{-1} (or 2,180 cm^{-1} at 1,023 K), which both gradually shift upward to about 2,192 cm^{-1} ($\theta \rightarrow 0$) can be observed. This envelope could be safely attributed to CO molecules interacting through the carbon-end with titanium sites present on the main (110) rutile facets (Jiang et al., 2018), which shows a peak centered at 2,181 cm^{-1} as previously observed on rutile micro-crystals (Mino et al., 2013).

While the weak band in the 2,160–2,150 cm^{-1} range is originated by the interaction of CO with residual OH groups located on corners, edges, and steps (Mino et al., 2013). Notice that the predominant feature is placed in the same spectral interval observed for anatase surfaces. Furthermore, the broad nature of the 2,182–2,180 cm^{-1} band (compare FWHM at θ = 1 insets in **Figures 3F,G**) is also indicative of the simultaneous presence of a few superimposed components, including (110) surface and some other minor features related to the less abundant exposed faces. The strong decrement of the overall intensity of the CO bands upon progressive activation at 973 K and at 1,023 K (**Figures 3F,G**) means that the formed rutile particles have very low surface area due to the known sintering effects (Mino et al., 2012). It is noteworthy that the band at 2,189 cm^{-1}, which is the most stable upon outgassing the CO from anatase, is totally absent. This can be explained with the complete conversion of anatase into the rutile phase. Another relevant observation comes from the inspection of **Figure 3G**. In this figure, the most abundant CO species on rutile (presumably adsorbed on the most extended faces and terraces) are found at frequencies (2,180–2,192 cm^{-1}) slightly higher than those of CO absorbed on the most abundant faces of anatase. This result is in agreement with the theoretical calculations of Scaranto and Giorgianni (2008). From this, it is inferred that the feature in the 2,180–2,192 cm^{-1} range is due to CO on (110) faces of rutile.

FTIR Spectra of ^{12}CO-^{13}CO Isotopic Mixture Adsorbed at the TiO_2 Surface Activated at 773 K

It is known that the FTIR spectra of different isotopes, co-adsorbed at the surface of many materials, can offer a valuable tool to distinguish the different types of the interactions inside the adlayer, thus highlighting the ultimate nature of the surface sites (Hadjiivanov et al., 2014). As a matter of fact, it is known that the dynamic interactions are due to dipole–dipole coupling between the adsorbed CO molecules, while the static interactions depend on the ability of the adsorbed molecules in transferring negative charges to the adjacent adsorption sites (Hammaker et al., 1965). From this, it comes out that the observed shifts induced by both dynamic ($\Delta\nu_{dyn}$) and static ($\Delta\nu_{st}$) interactions on oxide surfaces can give information on the surface sites. Briefly, when the dipolar molecules vibrate with the same frequency, dynamic interactions are observed. Therefore, the observed dynamic shift basically can be evaluated from the difference between ν (^{12}CO), when pure CO is adsorbed at high coverage and ν (^{12}CO)

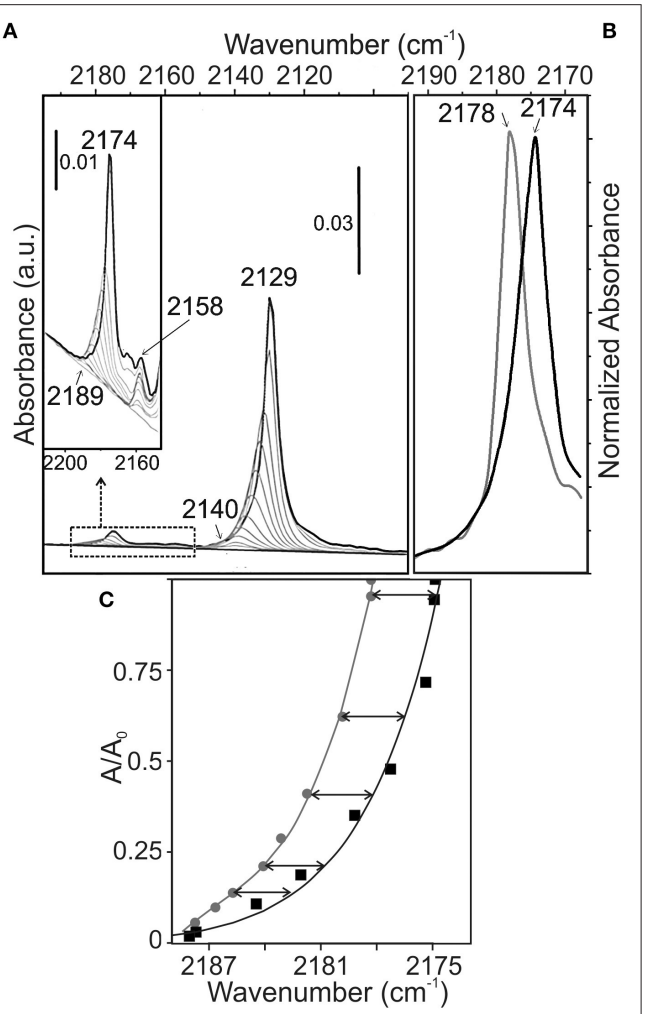

FIGURE 4 | FTIR spectra at 100 K of **(A)** adsorbed ^{12}CO-^{13}CO isotopic mixture (P_{CO} = 2.5 mbar and P_{13CO} = 50 mbar) at decreasing coverages on TiO_2 (P25) surface, previously outgassed at 773 K for 2 h and successively treated at the same temperature with static O_2 (P_{O2} = 50 mbar) for the same time, **(B)** comparison of adsorbed ^{12}CO-^{13}CO isotopic mixture (black line) with pure ^{12}CO (gray line) at maximum coverage on TiO_2 surface; **(C)** Relative IR absorbance vs. frequency value during desorption of CO from ^{13}CO-^{12}CO mixture (P_{CO} = 2.5 mbar and P_{13CO} = 50 mbar) (solid black line), and from ^{12}CO (P_{CO} = 50 mbar) (gray solid line).

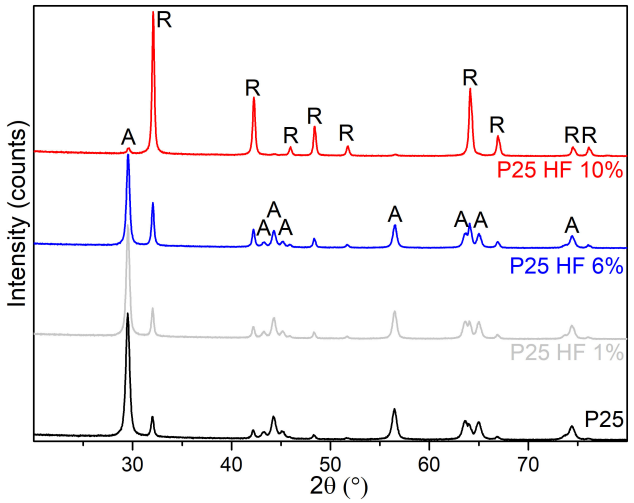

FIGURE 5 | XRD patterns of TiO_2 P25 etched with 1, 6, and 10 vol% HF solutions (gray, blue and red patterns, respectively) and compared with the XRD pattern of the native P25 powder (black pattern).

inside isotopic mixtures containing a small percentage of ^{12}CO (Hadjiivanov et al., 2014).

Coming to the interaction of CO molecules with P25 surfaces, $^{12}CO/^{13}CO$ isotopic mixture method was used to study dynamic and static interactions of the carbonyl bands that are shifting with the coverage. To this purpose, the contribution of the dynamic and static effects to the total shift ($\Delta\nu_{tot} = 11\ cm^{-1}$) observed on the P25 sample, previously outgassed at 773 K, can be calculated by comparing the spectra of ^{12}CO (about 99%) and $^{12}CO/^{13}CO$ (5:95) isotopic mixture (**Figures 4A–C**).

At full coverage, the band due to ^{12}CO molecules in the monolayer of the isotopic mixture is observed at 2,174 cm^{-1} instead of 2,178 cm^{-1} (**Figure 4B**). From this, the dynamic shift ($\Delta\nu_{dyn}$) can be calculated to be $+4\ cm^{-1}$, while a static shift ($\Delta\nu_{static}$) of $-15\ cm^{-1}$ is obtained (**Figures 4B,C**). The obtained shifts are similar to those found for CO adsorbed on other oxides (MgO, NiO, ZnO, δ-Al_2O_3, α-Fe_2O_3, etc.) (Hollins and Pritchard, 1980; Spoto et al., 1990; Zecchina et al., 1996).

XRD Analysis: Phase Composition and Crystal Sizes of TiO_2 P25 Treated With HF Etching Solutions

XRD patterns of P25 powders chemically treated with 1 or 6 vol% HF for 1 h, or 10 vol% HF for 12 h are shown in **Figure 5**.

The obtained phase compositions and crystal sizes are summarized in **Table 2**. From the XRD patterns it is clear that slight changes can be observed for the TiO_2 powder etched by diluted HF solution (1 vol%) for 1 h as compared with the native P25. Such differences become much more evident for the more concentrated HF solutions (6 vol% HF for 1 h and 10 vol % for 12 h). In the latter case, the remarkable anatase-to-rutile phase transition is shown, together with the progressive increasing of the crystal sizes (**Table 2**).

TABLE 2 | Phase composition and crystal size analysis from XRD patterns for the HF-etched TiO_2 samples shown in **Figure 5**.

Sample	Phase composition[a]		Crystallite sizes[b]	
	Anatase (wt%)	Rutile (wt%)	Anatase (nm)	Rutile (nm)
TiO_2 P25	83	17	28	47
P25 HF 1%-1 h	80	20	31	48
P25 HF 6%-1 h	67	33	33	49
P25 HF 10%-12 h	3	97	36	53

[a] *Calculated by Spurr and Myers relation (see experimental section).*
[b] *Calculated by Scherrer's equation (see experimental section).*

TEM and HRTEM Analysis: Structure and Morphology of the TiO_2 P25 Chemically Treated With HF Solutions

Due to the more remarkable changes of the structure and crystal sizes, samples chemically treated with the more severe etching conditions (6 vol% HF for 1 h and 10 vol% HF for 12 h solutions) have been TEM imaged (**Figure 6**).

Nanocrystals with sizes in the 10–40 nm range can be observed in the low-resolution TEM images (**Figures 6A,D**). HRTEM selected regions showed that nanoparticles are extremely crystalline in both samples. A nanocrystal of about 20 nm is HRTEM imaged in **Figure 6B**, where well-defined anatase (101) and (011) interference fringes are observed as obtained from the [1-11] zone axis, whose FFT image is shown in **Figure 6C**. The nanocrystal HRTEM imaged in **Figure 6E** exposes also well-defined interference fridges. Such fringes can be assigned to rutile (011) and (101) lattice planes as imaged from [−111] zone axis (**Figure 6F**). In conclusion, also for the HF-etched samples the observed lattice fringes are parallelly oriented to the external terminations of the nanocrystals, indicating that they preferentially expose (101) and (110) surfaces, as well as high-index (112) surfaces probably arising from the fluorine-mediated treatment (Yang et al., 2014). Newly developed {112} facets on both, anatase and rutile crystals, were also observed by Taguchi et al. (2003) by treatment with aqueous HF solutions. Furthermore, the different HF reactivity in dissolving anatase more easily than rutile was observed by Ohno et al. (2001b). Remarkably, the same authors also observed that, together with the isolation of pure rutile nanoparticles from TiO_2 P25, the rutile phase is not an overlayer on the surface of anatase particles, but it exists as separate phase from anatase particles (Ohno et al., 2001a).

FTIR Spectra of Adsorbed CO on TiO_2 Surfaces Etched by HF

FTIR spectra of CO adsorbed at 60 K on the surface of pristine and previously HF etched TiO_2 P25 samples (1, 6, and 10 vol% HF) activated at 773 K are reported in **Figures 7A–D**, respectively. The spectra have been acquired at 60 K, using a

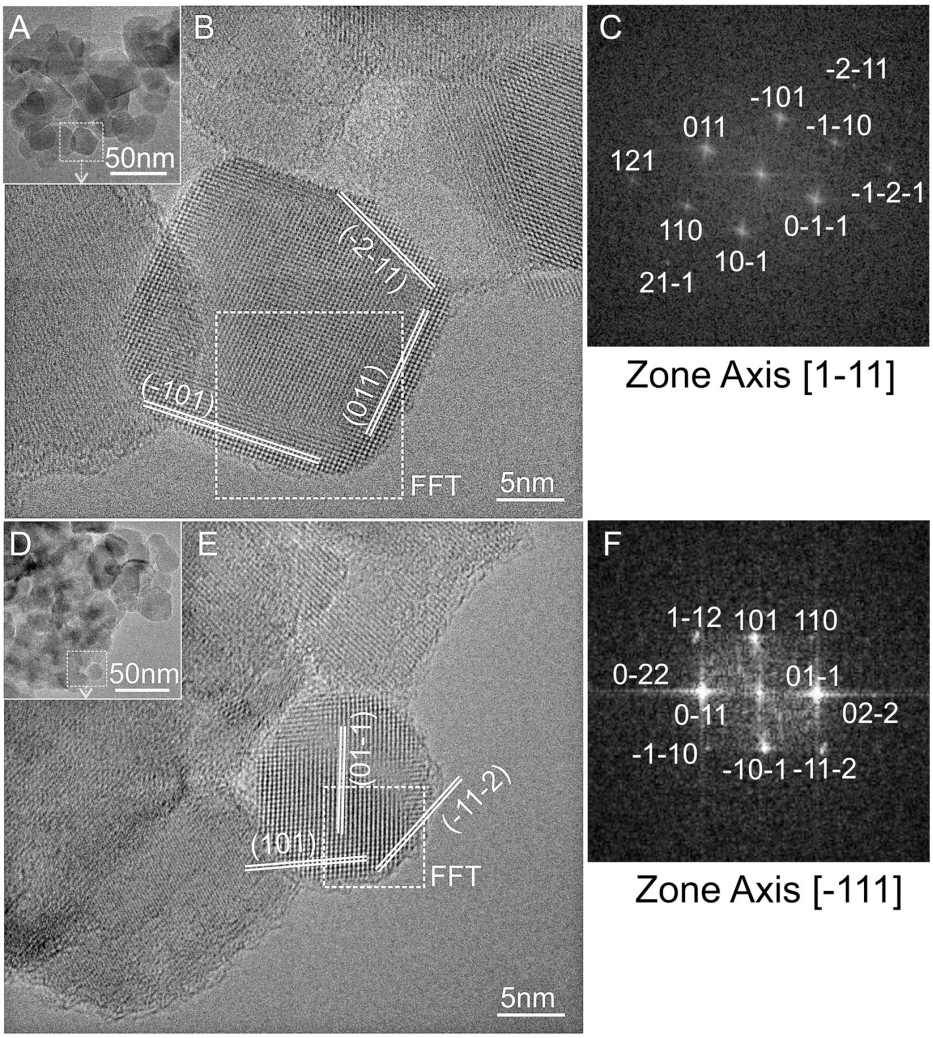

FIGURE 6 | TEM images and the related high-resolution TEM selected images of TiO_2 P25 etched with 6 vol% **(A,B)** and 10 vol% HF **(D,E)**; fast-Fourier-transform (FFT) images **(C,F)** of the nanocrystals selected in **(A,D)**, as obtained from [1-11] and [−111] zone axis directions, respectively.

cryostat (see Methods section), to better investigate the CO interaction with weak Ti^{4+} Lewis acid sites.

From the comparison of the more diluted HF-etched TiO_2 sample (1 vol% HF for 1 h, **Figure 7B**) with the native TiO_2 P25 (**Figure 7A**), both thermally activated at the same temperature, it is clear that the morphology has been scarcely modified, in agreement with the negligible changes in phase composition and mean crystallite size measured by XRD (see **Table 2**). With respect to the FTIR spectra of CO adsorbed at 100 K (**Figure 3**), we can note a better defined peak at 2,149 cm^{-1}, ascribed to the rutile phase (Mino et al., 2013), and an intense, broad and easily reversible band at 2,140 cm^{-1} due to a multilayer of physically adsorbed CO.

Increasing the HF concentration to 6 vol% results in a decrease of the intensity of the band at 2,165 cm^{-1}, ascribed to CO interacting with the (100) surface, and a parallel growth of the rutile signal at 2,149 cm^{-1} (**Figure 7C**). This finding is consistent with the increase of the rutile fraction from 20% to 33% (**Table 2**).

More drastic etching conditions (10 vol% HF for 12 h) lead to the almost complete dissolution of the anatase component, as confirmed by XRD analysis (**Figure 7D**) and (**Table 2**). The corresponding FTIR spectra are dominated by the signals ascribed to the rutile component centered at 2,149 cm^{-1}, already described above, and at 2,182 cm^{-1}. The latter band, observed also in the spectra of TiO_2 P25 treated at high temperatures (**Figures 3F,G**), is due to CO adsorbed on the (110) rutile surface. In the complex absorption in the 2,195–2,180 cm^{-1} range a residual contribution of the (101) and (110) anatase facets could also still be present. Conversely, the band at 2,165 cm^{-1}, associated to the (100) facets, completely disappears.

CONCLUSIONS

The surface modification of TiO_2 nanoparticles to design more effective photocatalysts is one of the major topics in

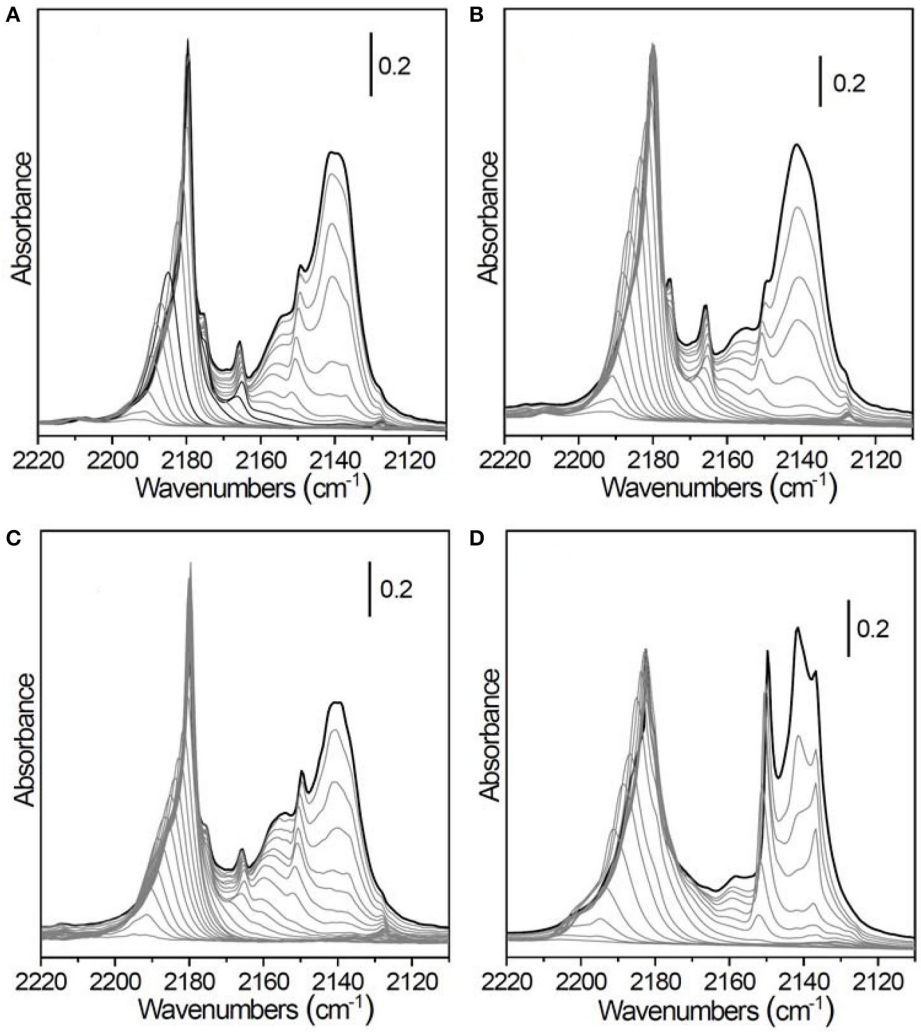

FIGURE 7 | FT-IR spectra, acquired at 60 K, of CO adsorbed at progressively decreasing coverages on TiO_2 P25 outgassed at 773 K for 4 h and previously etched in hydrofluoric acid: **(A)** pristine TiO_2 P25 (no HF treatment), **(B)** 1 vol% HF for 1 h, **(C)** 6 vol% HF for 1 h, **(D)** 10 vol% HF for 12 h.

photocatalysis. A multi-technique characterization approach, based on FTIR, TEM, and XRD analyses for the investigation of thermally/HF-chemically modified TiO_2 P25 powders has been shown in this contribution. Remarkably, FTIR studies of adsorbed CO are an effective method to investigate the surface sites structure, thus highlighting significant differences in the morphology and structure of different TiO_2 samples, coming from different thermal activations and etching processes by HF. In this context, FTIR spectra taken at decreasing CO coverage, at 100 K on TiO_2 P25 give rise to bands at 2,178 and 2,165–4 cm^{-1} due to carbonyls on Ti^{4+} sites of (101) and (100) facets. In addition, a band around 2,155 cm^{-1} can be explained with species adsorbed on surface hydroxyl groups and/or on the (001) anatase surface. Together with FTIR investigation, XRD, and TEM analyses were used to elucidate the role played by the thermal treatment (from RT to 1,023 K) and chemical etching by HF solutions (1 vol% for 1 h, 6 vol% for 1 h, 10 vol% for 12 h) in altering the phase composition and modifying the distribution of exposed surfaces of the pristine TiO_2 P25. FTIR spectra acquired at 60 K of samples obtained through more drastic etching conditions, are dominated by two components centered at 2,149 cm^{-1} and at 2,182 cm^{-1} due to CO adsorbed on the rutile phase, thus confirming the almost complete phase transition from anatase to rutile. The present study helps in the crystal and exposed facet engineering in the development of highly efficient photocatalysts.

DATA AVAILABILITY STATEMENT

The datasets generated for this study are available on request to the corresponding authors.

AUTHOR CONTRIBUTIONS

MU, FC, LM, and DS wrote and organized the manuscript. AC, TT, SC, GM, and AZ provided a substantial contribution to the work. All authors approved it for publication.

FUNDING

This work was supported by MIUR (Ministero dell'Istruzione, dell'Università e della Ricerca), INSTM Consorzio and NIS (Nanostructured Interfaces and Surfaces) Inter-Departmental Center of University of Torino.

REFERENCES

Byrne, C., Fagan, R., Hinder, S., Mccormack, D. E., and Pillai, S. C. (2016). New approach of modifying the anatase to rutile transition temperature in TiO_2 photocatalysts. *RSC Adv.* 6, 95232–95238. doi: 10.1039/C6RA19759K

Cesano, F., Agostini, G., and Scarano, D. (2015). Nanocrystalline TiO_2 micropillar arrays grafted on conductive glass supports: microscopic and spectroscopic studies. *Thin Solid Films* 590, 200–206. doi: 10.1016/j.tsf.2015.07.058

Cesano, F., Bertarione, S., Damin, A., Agostini, G., Usseglio, S., Vitillo, J. G., et al. (2008). Oriented TiO_2 nanostructured pillar arrays: synthesis and characterization. *Adv. Mater.* 20, 3342–3348. doi: 10.1002/adma.200702768

Cesano, F., Bertarione, S., Uddin, M. J., Agostini, G., Scarano, D., and Zecchina, A. (2010). Designing TiO_2 based nanostructures by control of surface morphology of pure and silver loaded titanate nanotubes. *J. Phys. Chem. C* 114, 169–178. doi: 10.1021/jp9087207

Cesano, F., Pellerej, D., Scarano, D., Ricchiardi, G., and Zecchina, A. (2012). Radially organized pillars of TiO_2 nanoparticles: synthesis, characterization and photocatalytic tests. *J. Photochem. Photob. A-Chem.* 242, 51–58. doi: 10.1016/j.jphotochem.2012.05.020

Chen, X., and Mao, S. S. (2007). Titanium dioxide nanomaterials: Synthesis, properties, modifications, and applications. *Chem. Rev.* 107, 2891–2959. doi: 10.1021/cr0500535

Cravanzola, S., Cesano, F., Gaziano, F., and Scarano, D. (2017). Sulfur-doped TiO_2: structure and surface properties. *Catalysts* 7:214. doi: 10.3390/catal7070214

Cravanzola, S., Sarro, M., Cesano, F., Calza, P., and Scarano, D. (2018). Few-layer MoS_2 nanodomains decorating TiO_2 nanoparticles: a case study for the photodegradation of carbamazepine. *Nanomaterials* 8:207. doi: 10.3390/nano8040207

Daoud, W. A., and Xin, J. H. (2008). Nucleation and growth of anatase crystallites on cotton fabrics at low temperatures. *J. Am. Ceram. Soc.* 87, 953–955. doi: 10.1111/j.1551-2916.2004.00953.x

Deiana, C., Fois, E., Coluccia, S., and Martra, G. (2010). Surface structure of TiO_2 P25 nanoparticles: IR study of hydroxy groups on coordinative defect sites supporting information. *J. Phys. Chem. C* 114, 21531–21538. doi: 10.1021/jp107671k

Deiana, C., Fois, E., Martra, G., Narbey, S., Pellegrino, F., and Tabacchi, G. (2016). On the simple complexity of carbon monoxide on oxide surfaces: facet-specific donation and backdonation effects revealed on TiO_2 anatase nanoparticles. *ChemPhysChem.* 17, 1956–1960. doi: 10.1002/cphc.201600284

Deiana, C., Minella, M., Tabacchi, G., Maurino, V., Fois, E., and Martra, G. (2013a). Shape-controlled TiO_2 nanoparticles and TiO_2 P25 interacting with CO and H_2O_2 molecular probes: a synergic approach for surface structure recognition and physico-chemical understanding. *Phys. Chem. Chem. Phys.* 15, 307–315. doi: 10.1039/C2CP42381B

Deiana, C., Tabacchi, G., Maurino, V., Coluccia, S., Martra, G., and Fois, E. (2013b). Surface features of TiO_2nanoparticles: combination modes of adsorbed CO probe the stepping of (101) facets. *Phys. Chem. Chem. Phys.* 15, 13391–13399. doi: 10.1039/c3cp51524a

Desjonqueres, M. C., and Spanjaard, D. (1996). *Concepts in Surface Physics*. Berlin: Springer. doi: 10.1007/978-3-642-61400-2

Diebold, U., Ruzycki, N., Herman, G. S., and Selloni, A. (2003). One step towards bridging the materials gap: surface studies of TiO_2 anatase. *Catal. Today* 85, 93–100. doi: 10.1016/S0920-5861(03)00378-X

Djaoued, Y., Badilescu, S., Ashrit, P. V., Bersani, D., Lottici, P. P., and Bruning, R. (2002). Low temperature Sol-Gel preparation of nanocrystalline TiO_2 thin films. *J. Sol-Gel Sci. Technol.* 24, 247–254. doi: 10.1023/A:1015305328932

Grissom, G., Jaksik, J., Mcenteec, M., Durke, E. M., Aishee, S. T. J., Cua, M., et al. (2018). Three-dimensional carbon nanotube yarn based solid state solar cells with multiple sensitizers exhibit high energy conversion efficiency. *Sol. Energy Mater. Sol. Cells* 171, 16–22. doi: 10.1016/j.solener.2018.06.053

Groppo, E., Lamberti, C., Cesano, F., and Zecchina, A. (2006). On the fraction of Cr-II sites involved in the C2H4 polymerization on the Cr/SiO2 phillips catalyst: a quantification by FTIR spectroscopy. *Phys. Chem. Chem. Phys.* 8, 2453–2456. doi: 10.1039/b604515d

Hadjiivanov, K., Mihaylov, M., Panayotov, D., Ivanova, E., and Chakarova, K. (2014). "Isotopes in the FTIR investigations of solid surfaces,"in *Spectroscopic Properties of Inorganic and Organometallic Compounds,* Vol, 45, eds, R. Douthwaite, S. Duckett, and J. Yarwood (Cambridge: Royal Society of Chemistry), 43–78. doi: 10.1039/9781782621485-00043

Hadjiivanov, K. I., and Klissurski, D. G. (1996). Surface chemistry of titania (anatase) and titania-supported catalysts. *Chem. Soc. Rev.* 25, 61–69. doi: 10.1039/cs9962500061

Hammaker, R. M., Francis, S. A., and Eischens, R. P. (1965). Infrared study of intermolecular interactions for carbon monoxide chemisorbed on platinum. *Spectrochim. Acta* 21, 1295–1309. doi: 10.1016/0371-1951(65)80213-2

Hanaor, D. A. H., and Sorrell, C. (2011). Review of the anatase to rutile phase transformation. *J. Mater. Sci.* 46, 855–874. doi: 10.1007/s10853-010-5113-0

Hollins, P., and Pritchard, J. (1980). Isotopic mixing for the determination of relative coverages in overlayer structures: CO on Cu (111). *Surf. Sci.* 99, 389–L394. doi: 10.1016/0039-6028(80)90387-8

Humayun, M., Raziq, F., Khan, A., and Luo, W. (2018). Modification strategies of TiO_2 for potential applications in photocatalysis: a critical review. *Green Chem. Lett. Rev.* 11, 86–102. doi: 10.1080/17518253.2018.1440324

Hussain, I., Chowdhury, A. R., Jaksik, J., Grissom, G., Touhami, A., Ibrahim, E. E., et al. (2019). Conductive glass free carbon nanotube micro yarn based perovskite solar cells. *Appl. Surf. Sci.* 478, 327–333. doi: 10.1016/j.apsusc.2019.01.233

Jain, S. M., Biedrzycki, J. J., Maurino, V., Zecchina, A., Mino, L., and Spoto, G. (2014). Acetylene oligomerization on the surface of TiO_2: a step forward in the in situ synthesis of nanostructured carbonaceous structures on the surface of photoactive oxides. *J. Mater. Chem. A* 2, 12247–12254. doi: 10.1039/C4TA01581A

Jaksik, J., Moore, H. J., Trad, T., Okoli, I. O., and Uddin, M. J. (2017). Nanostructured functional materials for advanced three-dimensional (3D) solar cells. *Solar Energy Mater. Solar Cells* 167, 121–132. doi: 10.1016/j.solmat.2017.03.033

Jia, S., Li, X., Zhang, B., Yang, J., Zhang, S., Li, S., et al. (2019). TiO_2/CuS heterostructure nanowire array photoanodes toward water oxidation: the role of CuS. *Appl. Surf. Sci.* 463, 829–837. doi: 10.1016/j.apsusc.2018.09.003

Jiang, F., Yang, L., Zhou, D., He, G., Zhou, J., Wang, F., et al. (2018). First-principles atomistic Wulff constructions for an equilibrium rutile TiO_2shape modeling. *Appl. Surf. Sci.* 436, 989–994. doi: 10.1016/j.apsusc.2017.12.050

Jiwei Ma, M., Li, W., and Dambournet, D. (2017). "Solution-based synthesis of nano-sized TiO_2 anatase in fluorinating media," in *Modern Synthesis Processes and Reactivity of Fluorinated Compounds*, eds. H. Groult, F. R. Leroux, and A. Tressaud (Amsterdam: Elsevier), 651–669. doi: 10.1016/B978-0-12-803740-9.00022-6

Kitano, M., Matsuoka, M., Hosoda, T., Ueshim, M., and Anpo, M. (2008). Effect of HF treatment on the activity of TiO_2 thin films for photocatalytic water splitting. *Res. Chem. Interm.* 34, 577–585. doi: 10.1163/156856708784795518

Likodimos, V. (2018). Photonic crystal-assisted visible light activated TiO_2 photocatalysis. *Appl. Catal. B Environm.* 230, 269–303. doi: 10.1016/j.apcatb.2018.02.039

Liu, G., Yu, J. C., Lu, G. Q., and Cheng, H. M. (2011). Crystal facet engineering of semiconductor photocatalysts: motivations, advances and unique properties. *Chem. Commun.* 47, 6763–6783. doi: 10.1039/c1cc10665a

Liu, Y., Du, Y. E., Bai, Y., An, J., Li, J., Yang, X., et al. (2018). Facile synthesis of {101}, {010} and [111]-faceted anatase-TiO_2 Nanocrystals derived from porous metatitanic acid H2TiO3 for enhanced photocatalytic performance. *ChemistrySelect* 3, 2867–2876. doi: 10.1002/slct.201800018

Mino, L., Cesano, F., Scarano, D., Spoto, G., and Martra, G. (2019). Molecules and heterostructures at TiO_2 surface: the cases of H_2O, CO_2, and organic and inorganic sensitizers. *Res. Chem. Intermed*. 45, 5801–5829. doi: 10.1007/s11164-019-04003-y

Mino, L., Ferrari, A. M., Lacivita, V., Spoto, G., Bordiga, S., and Zecchina, A. (2011). CO adsorption on anatase nanocrystals: a combined experimental and periodic DFT study. *J. Phys. Chem. C* 115, 7694–7700. doi: 10.1021/jp2017049

Mino, L., Pellegrino, F., Rades, S., Radnik, J., Hodoroaba, V.-D., Spoto, G., et al. (2018). Beyond shape engineering of TiO_2 nanoparticles: post-synthesis treatment dependence of surface hydration, hydroxylation, lewis acidity and photocatalytic activity of TiO_2 anatase nanoparticles with dominant {001} or {101} facets. *ACS Appl. Nano Mater*. 1, 5355–5365. doi: 10.1021/acsanm.8b01477

Mino, L., Spoto, G., Bordiga, S., and Zecchina, A. (2012). Particles morphology and surface properties as investigated by HRTEM, FTIR, and periodic DFT calculations: from pyrogenic TiO_2 (P25) to nanoanatase. *J. Phys. Chem. C* 116, 17008–17018. doi: 10.1021/jp303942h

Mino, L., Spoto, G., Bordiga, S., and Zecchina, A. (2013). Rutile surface properties beyond the single crystal approach: new insights from the experimental investigation of different polycrystalline samples and periodic DFT calculations. *J. Phys. Chem. C* 117, 11186–11196. doi: 10.1021/jp401916q

Mino, L., Spoto, G., and Ferrari, A. M. (2014). CO_2 capture by TiO_2 anatase surfaces: a combined DFT and FTIR study. *J. Phys. Chem. C* 118, 25016–25026. doi: 10.1021/jp507443k

Mino, L., Zecchina, A., Martra, G., Rossi, A. M., and Spoto, G. (2016). A surface science approach to TiO_2 P25 photocatalysis: an *in situ* FTIR study of phenol photodegradation at controlled water coverages from sub-monolayer to multilayer. *Appl. Catal. B-Environ*. 196, 135–141. doi: 10.1016/j.apcatb.2016.05.029

Nolan, N. T., Seery, M. K., and Pillai, S. C. (2009). Spectroscopic investigation of the anatase-to-rutile transformation of sol-gel-synthesized TiO_2 photocatalysts. *J. Phys. Chem. C* 113, 16151–16157. doi: 10.1021/jp904358g

Ohno, T., Sarukawa, K., and Matsumura, M. (2001a). Photocatalytic activities of pure rutile particles isolated from TiO_2 powder by dissolving the anatase component in HF solution. *J. Phys. Chem. B* 105, 2417–2420. doi: 10.1021/jp003211z

Ohno, T., Sarukawa, K., Tokieda, K., and Matsumura, M. (2001b). Morphology of a TiO_2 photocatalyst (Degussa, P-25) consisting of anatase and rutile crystalline phases. *J. Catal*. 203, 82–86. doi: 10.1006/jcat.2001.3316

Peng, Y. K., Chou, H. L., and Edman Tsang, S. C. (2018). Differentiating surface titanium chemical states of anatase TiO_2 functionalized with various groups. *Chem.Sci*. 9, 2493–2500. doi: 10.1039/C7SC04828A

Qadir, M. B., Li, Y., Sahito, I. A., Arbab, A. A., Sun, K. C., Mengal, N., et al. (2016). Highly functional TNTs with superb photocatalytic, optical, and electronic performance achieving record PV efficiency of 10.1% for 1D-based DSSCs. *Small* 2016, 4508–4520. doi: 10.1002/smll.201601058

Scarano, D., Bertarione, S., Cesano, F., Spoto, G., and Zecchina, A. (2004). Imaging polycrystalline and smoke MgO surfaces with atomic force microscopy: a case study of high resolution image on a polycrystalline oxide. *Surf. Sci*. 570, 155–166. doi: 10.1016/j.susc.2004.07.024

Scarano, D., Cesano, F., and Zecchina, A. (2019). MoS_2 domains on TiO_2-based nanostructures: role of Titanate/TiO_2 transformation and sulfur doping on the interaction with the support. *J. Phys. Chem. C* 123, 7799–7809. doi: 10.1021/acs.jpcc.8b06637

Scarano, D., Spoto, G., Bordiga, S., Zecchina, A., and Lamberti, C. (1992). Lateral interactions in CO adlayers on prismatic ZnO faces: a FTIR and HRTEM study. *Surf. Sci*. 276, 281–298. doi: 10.1016/0039-6028(92)90716-J

Scaranto, J., and Giorgianni, S. (2008). A quantum-mechanical study of CO adsorbed on TiO_2: a comparison of the Lewis acidity of the rutile (110) and the anatase (101) surfaces. *J. Mol. Struct.-Theochem*. 858, 72–76. doi: 10.1016/j.theochem.2008.02.027

Selloni, A. (2008). Anatase shows its reactive side. *Nat. Mater*. 7, 613–615. doi: 10.1038/nmat2241

Spoto, G., Morterra, C., Marchese, L., Orio, L., and Zecchina, A. (1990). The morphology of TiO_2 microcrystals and their adsorptive properties towards CO: a HRTEM and FTIR study. *Vacuum* 41, 37–39. doi: 10.1016/0042-207X(90)90264-Y

Spurr, R. A., and Myers, H. (1957). Quantitative analysis of anatase-rutile mixtures with an X-Ray diffractometer. *Anal. Chem*. 29, 760–762. doi: 10.1021/ac60125a006

Taguchi, T., Saito, Y., Sarukawa, K., Ohno, T., and Matsumura, M. (2003). Formation of new crystal faces on TiO_2 particles by treatment with aqueous HF solution or hot sulfuric acid. *New J. Chem*. 27, 1304–1306. doi: 10.1039/b304518h

Tamgadge, R. M., and Shukla, A. (2018). Fluorine-doped anatase for improved supercapacitor electrode. *Electrochimica Acta* 289, 342–353. doi: 10.1016/j.electacta.2018.09.034

Tsyganenko, A. A., Denisenko, L. A., Zverev, S. M., and Filimonov, V. N. (1985). Infrared study of lateral interactions between carbon monoxide molecules adsorbed on oxide catalysts. *J. Catal*. 94, 10–15. doi: 10.1016/0021-9517(85)90077-6

Uddin, M. J., Cesano, F., Bonino, F., Bordiga, S., Spoto, G., Scarano, D., et al. (2007). Photoactive TiO_2 films on cellulose fibres: synthesis and characterization. *J. Photochem. Photob. A-Chem*. 189, 286–294. doi: 10.1016/j.jphotochem.2007.02.015

Uddin, M. J., Daramola, D. E., Velasquez, E., Dickens, T. J., Yan, J., Hammel, E., et al. (2014). A high efficiency 3D photovoltaic microwire with carbon nanotubes (CNT)-quantum dot (QD) hybrid interface. *Phys. Status Solidi RRL* 8, 898–903. doi: 10.1002/pssr.201409392

Vittadini, A., Selloni, A., Rotzinger, F. P., and Grätzel, M. (1998). Structure and energetics of water adsorbed at TiO_2 anatase 101 and 001 surfaces. *Phys. Rev. Lett*. 81:2954. doi: 10.1103/PhysRevLett.81.2954

Wen, C. Z., Zhou, J. Z., Jiang, H. B., Hu, Q. H., Qiao, S. Z., and Yang, H. G. (2011). Synthesis of micro-sized titanium dioxide nanosheets wholly exposed with high-energy {001} and {100} facets. *Chem. Commun*. 47, 4400–4402. doi: 10.1039/c0cc05798c

Xu, M. C., Gao, Y. K., Moreno, E. M., Kunst, M., Muhler, M., Wang, Y. M., et al. (2011). Photocatalytic activity of bulk TiO_2 anatase and rutile single crystals using infrared absorption spectroscopy. *Phys. Rev. Lett*. 106:138302. doi: 10.1103/PhysRevLett.106.138302

Yang, H. G., Sun, C. H., Qiao, S. Z., Zou, J., Liu, G., Smith, S. C., et al. (2008). Anatase TiO_2 single crystals with a large percentage of reactive facets. *Nat. Mater*. 453, 638–641. doi: 10.1038/nature06964

Yang, S., Yang, B. X., Wu, L., Li, Y. H., Liu, P., Zhao, H., et al. (2014). Titania single crystals with a curved surface. *Nature Commun*. 5, 1–7. doi: 10.1038/ncomms6355

Zaera, F. (2014). New advances in the use of infrared absorption spectroscopy for the characterization of heterogeneous catalytic reactions. *Chem. Soc. Rev*. 43, 7624–7663. doi: 10.1039/C3CS60374A

Zecchina, A., Scarano, D., Bordiga, S., Ricchiardi, G., Spoto, G., and Geobaldo, F. (1996). IR studies of CO and NO adsorbed on well characterized oxide single microcrystals. *Catal. Today* 27, 403–435. doi: 10.1016/0920-5861(95)00202-2

Zhang, H., Wang, Y., Liu, P., Han, Y., Yao, X., Zou, J., et al. (2011). Anatase TiO_2crystal facet growth: mechanistic role of hydrofluoric acid and photoelectrocatalytic activity. *ACS Appl. Mater. Interf*. 3, 2472–2478. doi: 10.1021/am200363p

Zou, Y., Gao, G., Wang, Z., Shi, J. W., Wang, H., Ma, D., et al. (2018). Formation mechanism of rectangular-ambulatory-plane TiO_2 plates: an insight into the role of hydrofluoric acid. *Chem. Commun*. 54, 7191–7194. doi: 10.1039/C8CC02309C

Conflict of Interest: The authors declare that the research was conducted in the absence of any commercial or financial relationships that could be construed as a potential conflict of interest.